

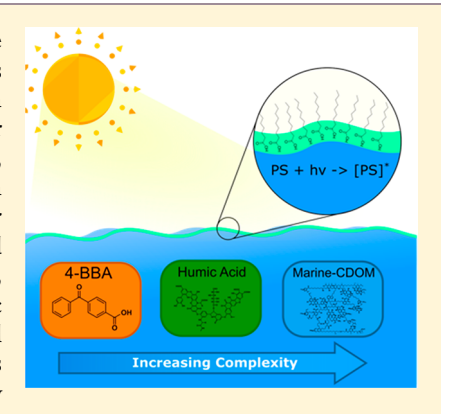
# Shedding Light on Photosensitized Reactions within Marine-Relevant Organic Thin Films

Jonathan V. Trueblood, †,‡ Michael R. Alves, †,‡ Dylan Power,‡ Mitchell V. Santander,‡ Richard E. Cochran,‡ Kimberly A. Prather,‡ and Vicki H. Grassian\*,‡,\$,||

<sup>‡</sup>Department of Chemistry and Biochemistry, <sup>§</sup>Scripps Institution of Oceanography, and <sup>II</sup>Department of Nanoengineering, University of California, San Diego, La Jolla, California 92093, United States

Supporting Information

ABSTRACT: Photochemical processes drive much of the daytime gas-phase chemistry in the atmosphere. Within condensed phases, such as aerosol particles and thin films enriched in organics, much less is understood about these processes. An investigation aimed at better understanding photosensitized reactions that can occur within marine-relevant condensed-phase systems is described herein. In particular, photosensitized reactions have been investigated between a fatty acid model system and different photosensitizers within thin organic films representative of molecular species found in the sea surface microlayer and sea spray aerosols. Photosensitized reactions of thin films containing nonanoic acid and three different photosensitizers, including 4-benzoylbenzoic acid, humic acid, and marine-derived dissolved organic matter, were probed using a suite of analytical techniques, including vibrational spectroscopy, excitation—emission matrix spectroscopy, and ultra-high-resolution mass spectrometry. Considerable differences were found in the photosensitizing capability for each of these systems. We also present an analysis of the molecular differences



between the different photosensitizers to explain their unique characteristics and light-absorbing properties. Overall, this study sheds light on the relevance of such reactions in the marine environment.

KEYWORDS: photochemistry, photosensitized reactions, marine-derived dissolved organic matter (m-DOM), sea surface microlayer (SSML), aerosols

# ■ INTRODUCTION

Air—water interfaces are ubiquitous throughout Earth, existing in lakes, oceans, and rivers and at the surface of aerosols. An important property of the air—water interface is its ability to concentrate certain surface-active chemical species relative to the underlying bulk water, thereby exposing them to unique conditions for chemical and physical processing. One such species found in elevated concentrations at air—water interfaces is dissolved organic matter (DOM), which is operationally defined as the organic matter content of natural water that passes through 0.45 or 0.22  $\mu$ m filters.

The portion of DOM that interacts with light ranging from  $\sim$ 300 to 800 nm, known as chromophoric dissolved organic matter (CDOM),<sup>2</sup> is particularly important because it can proceed through a variety of photochemical pathways upon excitation by irradiation. Specifically, intersystem crossing to an excited triplet state is an important photochemical pathway for CDOM.<sup>3</sup> As a result of its relatively long lifetime, photoexcited triplet-state CDOM is known to efficiently degrade and react with organic compounds and contaminants in the aqueous phase. Such reactions occur either directly through H-abstraction and charge-transfer reactions or indirectly through the formation of other photochemically produced reactive intermediate species (e.g., hydroxyl radicals,  $H_2O_2$ , peroxy radicals, and singlet oxygen), which then react with the organic

substrates.<sup>4,5</sup> In this manuscript, we define a reaction initiated by an excited-state molecule with a substrate molecule as a photosensitized reaction, irrespective of the exact mechansim. For reactions in the bulk phase, these have been extensively studied and are known to form various low-molecular-weight saturated alcohols, aldehydes, and ketones.<sup>6</sup>

Recent studies using simple CDOM mimics and model systems [e.g., 4-benzoylbenzoic acid (BBA) and commercial humic acid (HA)] and single-component organic substrates [e.g., nonanoic acid (NA) and octanol] placed at the air—water interface have highlighted the role of a previously unknown class of photosensitized reactions in the formation of unsaturated and functionalized volatile organic compounds (VOCs) and condensed-phase products, including hexene, hexenal, heptadiene, and octenal, among others. Photosensitized reactions are thought to serve as a source of secondary organic aerosol (SOA) precursors and are unique to the air—water interface as a result of its concentrating ability, allowing for efficient interaction between formed radical species.

Received: March 19, 2019 Revised: May 28, 2019 Accepted: May 29, 2019 Published: May 29, 2019



Because two-thirds of Earth is covered in oceans, photosensitized reactions may be of great importance either at the sea surface microlayer (SSML), which is known to be enriched with DOM, or within sea spray aerosol (SSA) produced at the SSML-air interface. Indeed, the total pool of DOM in marine environments (termed m-DOM) accounts for one of the largest carbon reservoirs on Earth (662 Pg). 11 Because a portion of this large m-DOM pool consists of light-absorbing chromophoric components, termed m-CDOM, there is an abundance of molecules available to potentially serve as photosensitizers in such regions. However, experiments investigating potential photosensitized reactions at marine interfaces have, to date, used simple photosensitizer model systems (e.g., BBA), leaving uncertainty in how effective m-DOM and its associated fraction of m-CDOM behaves as a photosensitizer in the SSML and SSA.

Currently, the main chromophores in m-CDOM remain poorly defined in comparison to their terrestrial counterparts. In addition to lignin phenols from terrestrial runoff, m-CDOM is thought to acquire its photoactive properties from aromatic amino acids and a large class of poorly defined marine humic substances produced by the microbial and photochemical processing of phytoplankton exudates. <sup>12,13</sup> Because of its unique formation mechanism and molecular structure (*vide infra*), m-CDOM is therefore expected to have different photochemical properties than the terrestrially derived HA and simple model systems used in previous studies investigating photosensitized reactions. <sup>6</sup> For this reason, more complex and authentic photosensitizing systems need to be analyzed to determine the relevance of these photosensitizers at the air—water interfaces of the SSML and SSA.

In this study, we compared the ability of three different photosensitizing systems in carrying out photosensitized reactions with NA at the air—water interface: (1) the simple model system molecule BBA, (2) commercially purchased HA, and (3) authentic m-DOM, which includes m-CDOM, grown from a phytoplankton lab culture. The goal of this study was to better understand the role of m-CDOM in this new class of photosensitizing reactions in hopes of better determining the relevancy of these reactions in the marine environment.

## EXPERIMENTAL METHODS

Chemicals and Production of m-DOM. NA, a fatty acid commonly found in the SSML and SSA, was used as the organic substrate. Three different systems of increasing complexity were used as photosensitizers: a well-known photosensitizer molecule BBA (Sigma-Aldrich), HA (Sigma-Aldrich), and authentic m-CDOM, as discussed below.

To produce authentic m-DOM, which contains m-CDOM, 3 L of seawater was taken from the Scripps Institution of Oceanography pier and placed into a large flask. The seawater was spiked with Guillard's f/2 medium to induce a phytoplankton bloom. A fluorescent tube (model 205457, Full Spectrum Solutions, with T8 format, color temperature of 5700 K, and 2950 lm) above the flask was used to promote the growth of phytoplankton. The progress of the phytoplankton bloom was occasionally monitored by measuring *in vivo* chlorophyll fluorescence using a hand-held fluorimeter (Aquafluor, Turner Designs).

After approximately 3–4 weeks, the m-DOM material was extracted on the basis of a styrene divinylbenzene polymer (PPL) solid-phase extraction (SPE) procedure described previously.<sup>14</sup> Briefly, the acidified cultured seawater (pH 2)

was filtered first with 0.7  $\mu$ m Whatman glass filter (GF/F), followed by a 0.2  $\mu$ m GTTP filter to remove organisms and particulate matter. The SPE cartridges were pre-rinsed once with methanol, 3 times with dilute acid, 3 times with Milli-Q water, and 3 times with methanol. Filtered seawater was then passed through the SPE cartridges, followed by further rinsing with dilute acid 3 times (0.01 M HCl) and Milli-Q water 3 times and then dried under N<sub>2</sub>. m-DOM was then extracted from the SPE cartridge by eluting 3 times with methanol. The m-DOM methanol solution was then placed in a rotovap, and the dried sample was stored in a freezer.

Total Organic Carbon (TOC) Analysis. To aid in comparison of HA and m-DOM, aliquots of each sample in Milli-Q water were sent to Nelson Laboratories (Salt Lake City, UT, U.S.A.) for TOC analysis. A solution of 3.5 mg/mL HA in methanol was prepared and sonicated for 10 min. A total of 500  $\mu$ L of the HA/methanol solution was then extracted, evaporated, and then reconstituted in 40 mL of Milli-Q water. For TOC analysis of m-DOM, 5 mL of methanol was mixed with the dry m-DOM sample and sonicated for 10 min and then 500  $\mu$ L was extracted, evaporated, and reconstituted with 40 mL of Milli-Q water. Both solutions were further sonicated for 10 min after the addition of H<sub>2</sub>O and sent to Nelson Laboratories for TOC analysis.

Analysis of Photosensitized Reactions with NA. Attenuated Total Reflection Fourier Transform Infrared Spectroscopy (ATR-FTIR). ATR-FTIR was used to monitor the condensed phase of irradiated and non-irradiated NA in the presence of various photosensitizer systems. A LCS-100 solar simulator (model 94011A, Oriel) equipped with an AM1.5G filter to simulate solar output and a water filter to block infrared radiation was used to irradiate the systems. To mimic the organic-rich interface of the SSML and SSA particles, 400 µL of NA was placed on top of a thin film of photosensitizer that was formed on the surface of an amorphous material transmitting infrared radiation (AMTIR) crystal. The thin photosensitizer films were made by first creating a solution of the photosensitizer species in ethanol, 15.9 M for BBA, 3500 mg/L for HA, or 136.8 mg of C/L based on TOC analysis, and reconstituting the m-DOM in 5 mL of ethanol for a concentration of 640 mg of C/L. A total of 450  $\mu$ L of the photosensitizer/ethanol solution was then placed onto the AMTIR crystal, and dry air was passed over it for ~60 min to ensure solvent evaporation. Evaporation was assumed complete when subsequent ATR-FTIR scans revealed no further spectral changes or contributions from ethanol.

After evaporation of ethanol and formation of the photosensitizer thin film, 400  $\mu$ L of NA was placed on top of the thin photosensitizer film. To reduce evaporative losses, the AMTIR crystal was then covered using a trough plate fitted with an ultraviolet (UV) port window to allow light onto the sample. After 10 min of equilibration time, the solar simulator was either turned on for irradiation experiments or remained off for non-irradiation experiments. Spectra were then collected every 10 min for the next 60 min. At a spectral resolution of 8 cm<sup>-1</sup>, 128 scans were averaged across the spectral range of 800–4000 cm<sup>-1</sup>. After each experiment, the crystal was visually inspected to ensure the thin film of the photosensitizer had not been removed from the crystal interface by dissolution in the NA medium. While it is still possible that small amounts of photosensitizer were dissolved into solution, we do not expect

large differences in the resulting spectra because the penetration depth of the evanescent beam ( $\sim$ 1  $\mu$ m) was still large enough that it would interrogate the photosensitizer in solution phase.

Ultra-High-Resolution Mass Spectrometry of Reaction Products. To tentatively identify the organic products formed during the light and dark reactions, the solution from the AMTIR crystal was extracted, stored at −20 °C, and then analyzed via an ultraperformance liquid chromatography tandem heated electrospray ionization-linear ion trap Orbitrap high-resolution mass spectrometer (UPLC-HESI-LIT-Orbitrap, Thermo Fisher Scientific) as adopted from Tinel et al. 10 In brief, samples were separated using a reverse-phase Hypersil GOLD aQ column (3  $\mu$ m, 50  $\times$  2.1 mm, Thermo Fisher Scientific) using a gradient elution method with mixtures of acetonitrile (Optima grade, Thermo Fisher Scientific) and water (ultrapure), each containing 0.1% formic acid (Optima grade, Thermo Fisher Scientific). Peaks were detected in both positive and negative modes at a capillary voltage set to 2.8 and 3.2 kV for negative and positive modes, respectively, with the electrospray needle and capillary maintained at 325 °C. The HESI gases were set as follows (arbitrary units): sheath at 30, auxiliary at 10, and sweep at 0. HESI-LIT-Orbitrap was mass-calibrated the day of sample analysis for each experiment, using pre-made mixtures specific to positive and negative ionization modes (Pierce ESI Ion Calibration Solutions, Thermo Fisher Scientific) and maintaining mass accuracies of <2 ppm mass error. With these solutions, mass calibration was performed in the ranges of m/z195-1921 and 265-1986 for positive and negative ionization modes, respectively. All data acquisitions were performed with the mass range set to m/z 80-2000 and the mass resolution set to 120 000. Samples run in positive mode were derivatized with O-(2,3,4,5,6-pentafluorobenzyl)hydroxylamine (PFBHA) prior to analysis to effectively identify organic products containing aldehyde and ketone in a manner similar to Tinel and co-workers. 10 Samples run in negative mode were not derivatized. All extracts were prepared by diluting 25  $\mu$ L of the sample to 1 mL with a 1:1 acetonitrile/water mixture. Aliquots were then analyzed after a 24 h period.

Analyses of Photosensitizers. Ultra-High-Resolution Mass Spectrometry. To determine the chemical structure and, hence, better understand the photochemical properties of complex photosensitizers (HA and m-DOM), ultra-highresolution mass spectrometry was again used. Extracts of each photosensitizer were introduced into a HESI-LIT-Orbitrap mass spectrometer via direct injection at a flow rate of 5  $\mu$ L min<sup>-1</sup>, with the electrospray needle maintained at 50 °C and the capillary at 325 °C. The HESI gases were set as follows (arbitrary units): sheath at 5, auxiliary at 0, and sweep at 0. While it was understood that ionization suppression could potentially limit the observation and identification of many species with the DOM sample, chromatographic separation was not used in this case as a result of the difficulty in separating components in DOM, which is known to contain tens of thousands of unique molecular species.

Using the ability of HESI–LIT–Orbitrap MS to separate complex mixtures, thousands of molecular signatures were still detected. Molecular formula assignments were performed using the Xcalibur (Thermo Fisher Scientific) software with the following element ranges: <sup>12</sup>C, 0–30; <sup>1</sup>H, 0–50; <sup>16</sup>O, 0–30; <sup>14</sup>N, 0–5; <sup>32</sup>S, 0–2; and <sup>23</sup>Na, 0–1 (sodium adduct for positive mode species only). Compositions including phos-

phorus (P) were excluded in this analysis as a result of the uncertainty of their presence in our samples.  $^{15,16}$  Formulas with a relative double bond greater than 15 and/or with an O/C ratio less than 0 or greater than 2.5 were rejected. Additionally, peaks were chosen with a mass error of less than 5 ppm and with a relative intensity greater than 0.05% of the largest detected peak. The majority of ions in both photosensitizers (HA and m-DOM) were found in positive mode, and the previously stated parameters set for composition analysis resulted in  $\sim$ 40–66% of ions being successfully characterized for both modes.

Assigned formulas were then categorized by compound class based on elemental stoichiometries as performed previously.  $^{17}$  The modified aromaticity index (AI $_{\rm mod}$ ) was calculated according to eq 1

$$AI_{mod} = (1 + C - 0.5O - S - 0.5H)/(C - 0.5O - S - N - P)$$
(1)

where P = 0 for our identified compounds. Compound classes were then identified as follows: aromatic,  $AI_{mod} = 0.5-0.67$ ; condensed aromatic,  $AI_{mod} > 0.67$ ; highly unsaturated,  $AI_{mod} < 0.5$  and H/C < 1.5; aliphatic, HC = 1.5-2.0, O/C < 0.9, and N = 0; and peptide, H/C = 1.5-2.0, O/C < 0.9, and N > 0. As noted in previous work, compounds identified as peptides have molecular formulas of peptides but the actual structure may differ. <sup>17</sup>

Fluorescence Excitation—Emission Matrices (EEMs). Fluorescence EEMs of HA and m-DOM were obtained using a spectrofluorometer (Aqualog with extended range, Horiba Scientific). Dry samples were resuspended in 5 mL of ultrapure water. A small aliquot (1.5 mL) was then used to obtain EEMs. Excitation wavelengths ranged from 235 to 450 nm. Emission wavelengths ranged from 250 to 800 nm. A background spectrum acquired with ultrapure water was then subtracted from all EEMs. EEMs were corrected for inner-filter effects based on absorbance spectra measured simultaneously. Finally, Rayleigh scattering (first and second order) was removed.

# ■ RESULTS AND DISCUSSION

Analysis of Photosensitized Reactions for Three Different Photosensitizers. Analysis of products formed during irradiated and non-irradiated NA with three different photosensitizers was conducted using ATR-FTIR spectroscopy and UPLC-HESI-LIT-Orbitrap MS. As mentioned, a thin film of the photosensitizer was first formed on an AMTIR ATR-FTIR crystal. Individual spectra for each of the three photosensitizers are shown in Figure S1 of the Supporting Information. After creation of the photosensitizer thin film, NA was placed on top. The full signal spectrum of each photosensitizer with the NA system is largely dominated by NA (also shown in Figure S2 of the Supporting Information).

After preparation of the NA and photosensitizer thin film, the system was then either kept in the dark for 1 h or irradiated with a solar simulator, with spectra collected every 10 min. Panels A–C of Figure 1 show select regions of ATR–FTIR difference spectra (final–initial) for irradiated and non-irradiated NA in the presence of all three photosensitizers as a function of time over 1 h. Increasingly bright colored lines correspond to increasing irradiation time, while gray lines show the difference spectra for samples kept in the dark (i.e., no irradiation). Control experiments in which only either NA or m-DOM was irradiated are shown in Figure S3 of the

Table 1. Signal Strength and Enrichment Ratios for Select Products as Detected by MS Analysis for Samples of Various Photosensitizers in the Presence of NA

molecular formula	assigned structure	irradiated BBA	BBA light/dark <sup>a</sup>	irradiated HA	HA light/dark <sup>a</sup>	irradiated m-DOM	m-DOM light/darl
			Combination 1	Products	-		-
$C_{23}H_{28}O_5$	NA + BBA	strong	>200000	below threshold	NA	below threshold	NA
$C_{18}H_{34}O_4$	2NA – 2H	medium	>100	below threshold	NA	medium	0.92
0, ,			Carboxylic .	Acids			
$C_8H_{16}O_2$	octanoic acid	medium	>200000	medium	1.07	strong	1.02
$C_8H_{14}O_2$	octenoic acid	weak	>10000	below threshold	NA	below threshold	NA
$C_9H_{16}O_2$	nonenoic acid	weak	>10000	below threshold	NA	below threshold	NA
$C_7H_{14}O_2$	heptanoic acid	weak	1.5	medium	1.09	medium	1.02
			Oxygenated	Acids			
$C_9H_{16}O_3$	oxo-NA	strong	42.81	strong	1.11	strong	0.93
$C_9H_{16}O_4$	hydroxy-oxo-NA	medium	22.27	strong	1.01	strong	0.99
$C_9H_{18}O_3$	hydroxy-NA	medium	5.77	strong	1.07	strong	1.12
$C_6H_{10}O_4$	hydroxy-oxo-octanoic acid	medium	1.73	strong	1.02	medium	1.02
			Aldehydes/K	etones			
$C_7H_{12}O_2$	heptanedial	weak	11.53	below threshold	NA	below threshold	NA
$C_6H_{10}O_2$	hexanedial	weak	7.75	below threshold	NA	below threshold	NA
$C_8H_{14}O$	octenal	strong	3.26	medium	0.99	strong	1
$C_9H_{16}O$	nonenal	weak	2.14	below threshold	NA	weak	0.96
$C_8H_{16}O$	octanal	strong	1.79	medium	9828.14	strong	1.04
$C_9H_{16}O_2$	nonanedial	medium	1.21	medium	1.26	strong	0.99
$C_9H_{18}O$	nonanal	weak	1.2	weak	0.48	strong	0.71
$C_6H_{10}O$	hexenal	medium	1.19	weak	1.24	medium	0.97
$C_7H_{14}O$	heptanal	weak	1.17	below threshold	NA	medium	1.04
$C_6H_{12}O$	hexanal	medium	1.1	below threshold	NA	below threshold	NA
$C_5H_8O$	pentenal	below threshold	NA	medium	1.26	below threshold	NA

<sup>&</sup>lt;sup>a</sup>Light/dark refers to the ratio between irradiated and non-irradiated samples.

Supporting Information. After irradiation and analysis by ATR-FTIR, samples were extracted, derivatized, and analyzed using UPLC-HESI-LIT-Orbitrap MS for identification of specific molecular species. Table 1 shows signal strength and ratio (irradiated/non-irradiated) of counts of select products found upon analysis in positive and negative modes, separately. It is should be noted that the analysis of mixtures via highresolution mass spectrometry (HRMS) ESI is not entirely quantitative as a result of differences in ionization efficiencies of the samples. To comparatively assess the photochemical production of identified species between experiments, four thresholds relative to the signal of the total ion count (TIC) spectra of HRMS were calculated and used to create four categories to describe the relative intensities of each product. The categories were assigned in a manner similar to previous studies<sup>18</sup> and are calculated as follows: First, "below threshold" was determined as 10 times greater than the average noise for that system. The following three categories (termed "weak", "medium", and "strong") were then each identified as being an order of magnitude higher than the previous threshold. For example, for the system of NA in the presence of BBA, the noise average was 10<sup>2</sup> counts, giving a "below threshold" value of 10<sup>3</sup> counts. "Weak" signals then had intensities greater than 10<sup>4</sup> counts; "medium" signals had intensities greater than 10<sup>5</sup> counts; and strong signals had intensities greater than 10<sup>6</sup> counts. Light/dark ratio counts were also calculated, indicating the extent to which irradiation produced observed products. Graphs showing ion counts for each system as well as water blanks in irradiated and non-irradiated conditions are shown in Figure S4 of the Supporting Information. An in-depth discussion of the findings for each system is given below.

BBA and NA. Figure 1A shows the difference spectra in the spectral region extending from 1300 to 1500 cm<sup>-1</sup> and the region from 3200 to 3500 cm<sup>-1</sup> for BBA and NA. Considering the expected products based on previous results in the literature, we attribute the broad negative absorption at ~1310 cm<sup>-1</sup> in the difference spectrua to the C-O stretching mode of NA. 19-21 The positive absorption with a maximum at 1399 cm<sup>-1</sup> is attributed to a combination of C-H bending and O-H in-plane bending from the formation of aldehydes and other oxygenated species.<sup>21</sup> The negative absorption centered at 1430 cm<sup>-1</sup> is due to the loss of O-H in-plane bending modes of NA.<sup>20,21</sup> It should be noted that this peak also overlaps with a peak in the BBA spectrum (Figure S1 of the Supporting Information). It is possible that the formation of combination products of BBA with various radicals may potentially be responsible for some of the changes seen here in the wavenumber.

The growth of two absorptions at 1633 and 1663 cm<sup>-1</sup> are assigned to C=C and C=O stretching modes, respectively, of unsaturated aldehydes.<sup>22</sup> The negative absorption at 1701 cm<sup>-1</sup> is due to the loss of C=O groups as NA is reacted away and consumed. Other positive absorptions in the difference spectra from 1710 to 1800 cm<sup>-1</sup> are most likely due to C=O stretches as a result of the formation of multiple aliphatic ketone/aldehyde species.<sup>21</sup> It is possible that these peaks are also caused by changes in the hydrogen-bonding state of NA. Loss of carboxylic acid dimers as a result of hydrogen bond disruption has been shown to cause the C=O peak to increase in wavenumber.<sup>20</sup> It is possible that, even with an infrared (IR) filter in place, irradiation of the sample by the solar simulator may cause changes in the hydrogen bonding state. However, in

light of the other changes to the spectra, it is clear that changes in the spectra are not exclusively a result of changes in the hydrogen bonding state but in fact due to photosensitized reactions. Finally, further evidence for the formation of oxygenated species is seen in the broad positive band caused by O–H stretching, with absorptions at 3333 and 3381 cm<sup>-1</sup>.

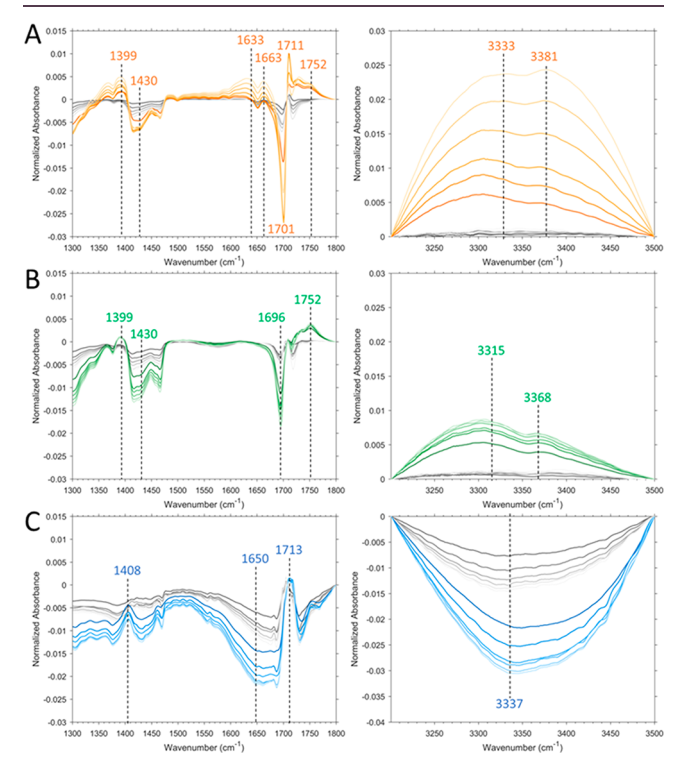


**Figure 1.** Select spectral regions of the ATR-FTIR difference spectra (final-initial) following 60 min of non-irradiated (gray lines) and irradiated (colored lines) NA in the presence of (A) BBA, (B) HA, and (C) m-DOM. Spectra were collected every 10 min. Lines become increasingly light with increased time.

The data from MS analysis of BBA and NA (Table 1) agree with the results from ATR-FTIR. The signal strength in the mass spectra following irradiation in conjunction with the light/dark ratio gives an indication as to which products were most abundant and whether they were formed through thermal dark reactions or light-induced reactions. The combination product NA plus BBA had a strong signal and was produced as a result of irradiation. Several identified saturated and unsaturated fatty acids (e.g., octenoic, nonenoic, and heptanoic acids) had weak to medium signal. Despite this, their signal was greatly enhanced relative to the dark experiments. Finally, oxygenated C<sub>8</sub>/C<sub>9</sub> acids as well as saturated and unsaturated C<sub>8</sub> ketones/aldehydes exhibited strong signals in both irradiated and non-irradiated samples, but their production clearly increased significantly upon irradiation, with production ratios ranging from 3.3 for octenal and 1.8 for octanal to 43 for oxo-NA. Overall, these results, showing the strong production of saturated and unsaturated oxygenated species with minimal production of carboxylic acids from the mixture of NA and BBA, are in agreement with previous studies.<sup>10</sup>

HA and NA. The products formed upon irradiation of the more complex system consisting of HA with NA were also examined with ATR-FTIR and MS. Figure 1B shows the ATR-FTIR difference spectra for samples that have been

irradiated in comparison to those that have not been irradiated for 1 h. Similar to that observed for NA in the presence of BBA, Figure 1B shows that following irradiation of NA and HA: there are positive absorptions near 1401 cm<sup>-1</sup>, which are assigned to bending modes of aldehydic C-H and O-H product functional groups.<sup>21</sup> Negative absorptions in the difference spectra are due to the loss of NA. Figure 1B also shows a negative absorption in the difference spectra at 1696 cm<sup>-1</sup> as a result of the loss of C=O stretching groups associated with NA and a positive absorption centered at 1752 cm<sup>-1</sup> as a result of the C=O stretching mode for aldehyde and ketone products. In contrast to NA with BBA results, NA mixed with HA has much smaller changes observed in the C= C and C=O stretching motion region from 1630 to 1660 cm<sup>-1</sup>, indicating less efficiently in producing unsaturated products. Finally, Figure 1B shows a broad band from 3100 to 3500 cm<sup>-1</sup> as a result of the stretching vibration of newly formed OH groups.

Table 1 shows the strength of the signal and ratio of counts, irradiated/non-irradiated, for select products from MS analysis of the system consisting of NA in the presence of HA. As expected, the BBA + NA combination product ion is absent. Signals from carboxylic acids are only slightly elevated following irradiation (for octanoic acid, 1.1 ratio of irradiated/non-irradiated, and for heptanoic acid, 1.1 ratio of irradiated/non-irradiated). Interestingly, the ketone/aldehyde with the greatest signal in the irradiated samples relative to the non-irradiated samples is octanal (9828), with lower values for nonanedial (1.3) and hexenal (1.2) and no enhancement for octenal (0.99). This perhaps indicates that a specific pathway is favored for NA mixed with HA. Finally, the production of oxygenated acids is favored only slightly in irradiated systems, with oxo-NA at 1.1 and hydroxy-NA also at 1.1. Overall, HA is a less efficient photosensitizer compared to BBA.

m-DOM and NA. ATR-FTIR difference spectra of m-DOM and NA in Figure 1C show that m-DOM appears to give much less condensed-phase products upon irradiation, as indicated by the weaker intensity negative absorptions in the difference spectra. Figure 1C has no positive absorptions and, instead, features only a broad decrease at 1650 cm<sup>-1</sup>. Given the complicated chemical nature of m-DOM, this peak could be due to any number of functional groups and their combinations within m-DOM, including C=C, C=O, N= C, and N-H. The absorption at 1713 cm<sup>-1</sup> does not change in a time-dependent manner and is likely due to the presence of NA, which does not appear to be clearly decreasing. The negative feature near 1730 cm<sup>-1</sup> indicates the loss of C=O species within the m-DOM. Furthermore, the large broad negative absorption centered at 3337 and 1430 cm<sup>-1</sup> in Figure 1C indicates the loss of O-H species. Overall, the ATR-FTIR spectra show losses in Figure 1C that may indicate that m-DOM could be undergoing direct photolysis and subsequent evaporation of low-volatility products. Difference spectra of an irradiated thin film of m-DOM (without NA coating) verified that m-DOM does undergo direct photochemistry (Figure S3 of the Supporting Information).

Ion counts in Table 1 show little to no enhancement in irradiated m-DOM and NA relative to non-irradiated samples for most products. Indeed, many systems feature an irradiated/non-irradiated ratio of ~1 or less than 1, including octenal and octanal, which were highly enhanced in systems containing either BBA or HA. The overall findings therefore are that BBA is an efficient photosensitizer, producing oxygenated species

# Scheme 1. Proposed Mechanism for the Reaction of NA with Various Photosensitizers: BBA, HA, and m-DOM<sup>a</sup>

"All products shown were present when BBA is the photosensitizer. Products highlighted in green and blue are seen with HA and m-DOM as the photosensitizer, respectively. The reaction pathway was modified from Tinel et al. 10

and unsaturated ketones/aldehydes, HA is a photosensitizer to a lesser extent, while the m-CDOM within m-DOM appears to exhibit little to no photosensitized reaction with the NA substrate. It should be noted that ATR—FTIR is limited to the analysis of the condensed-phase procuts and, therefore, is not probing gas-phase products that may form upon irradiation. Furthermore, differences between the spectra of irradiated m-DOM with NA and m-DOM by itself were observed and are indicative of potentially more complicated processes involved. Future studies are therefore needed to investigate the photochemical reactivity of m-DOM both by itself and in the presence of other organic matter species and in aqueous phase as well as any gas-phase products that may form.

From these results, a general mechanism for the photosensitized reaction of NA with various photosensitizer molecules is modified from previous studies of just BBA (Scheme 1). The reaction begins with H abstraction of the photosensitizer, leading to the addition of molecular oxygen or radical—radical interactions. Dependent upon the photosensitizer used, different pathways were more important. For example, disproportionation reactions leading to unsaturated fatty acid (nonenoic acid) or unsaturated aldehydes (i.e., octenal) were relevant only for BBA, while the pathways leading to saturated aldehydes and oxygenated species were more relevant for HA. The differences in reaction pathways and products observed are likely due to the molecular properties of each photosensitizer, which are discussed in the following section.

Comparison of m-DOM and HA: Molecular Composition and Chromophores. To better understand the

differences between HA and m-DOM as they compare to BBA, we conducted a series of experiments to better understand their molecular structure and associated chromophores.

EEMs. Panels A and B of Figure 2 show the EEM spectra of HA and m-DOM. Figure 2A has an EEM spectrum that has a

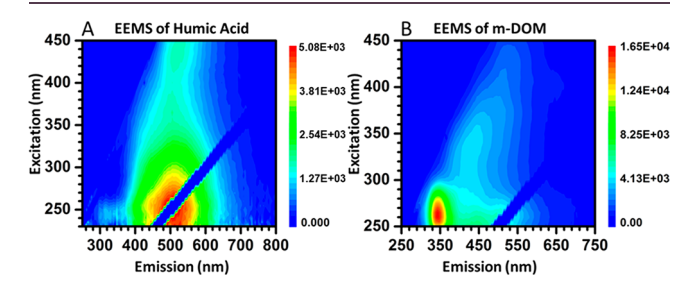


Figure 2. EEMs of (A) HA and (B) m-DOM.

main peak at  $\lambda_{\rm ex}/\lambda_{\rm em}=250/500$  nm that stretches into higher excitation wavelengths up to 450/500 nm. This spectrum is representative of HA extracted from terrestrial sources. Furthermore, the excitation at longer wavelengths is indicative of highly aromatic species. The EEM spectrum for m-DOM shown in Figure 2B has a peak at  $\lambda_{\rm ex}/\lambda_{\rm em}=250-280/350$  nm and a band that stretches to higher excitation wavelengths from 300 to 400/450 nm. A comparison of this to the literature 13 reveals that m-DOM contains proteins and marine humic substances with a lesser degree of aromaticity relative to terrestrial HA.

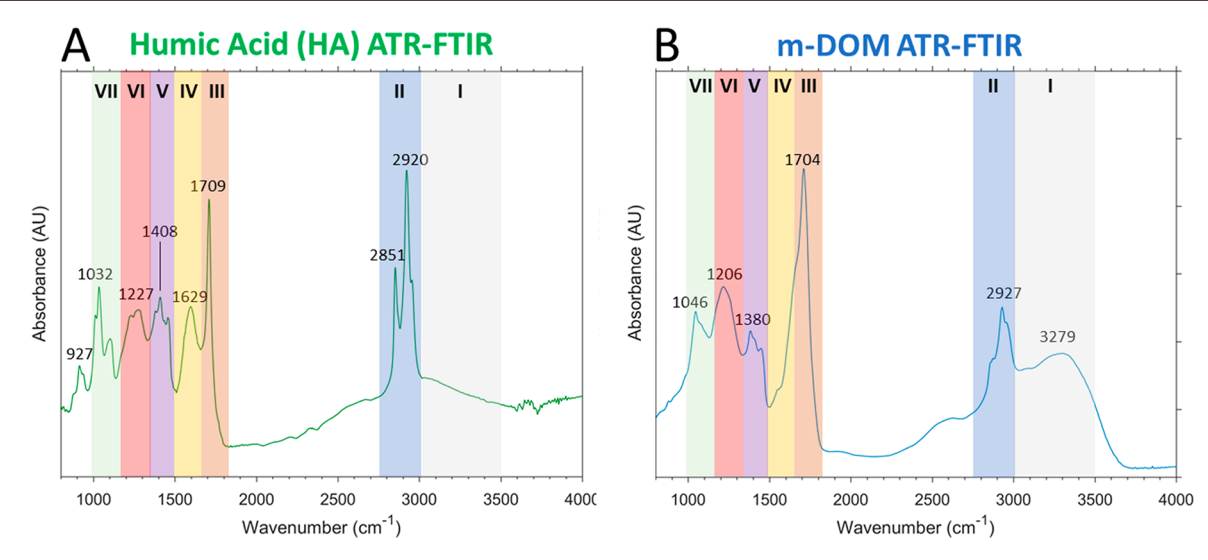


Figure 3. ATR-FTIR spectrum of (A) HA and (B) m-DOM extracted from a lab-grown phytoplankton culture. Peak assignments are listed in Table 2 according to the different regions labeled I-VII from high to low wavenumbers.

ATR-FTIR. Panels A and B of Figure 3 show the ATR-FTIR spectra of HA and m-DOM, respectively. As a result of the complex nature of these systems, the resulting spectra are broad, with each peak likely a composite of multiple functional groups. For this reason, a broad description of each region, labeled I-VII from high to lower wavenumbers, is given, with possible assignments for each of the absorptions in each region provided in Table 2.

Table 2. Peak Assignments of ATR-FTIR Spectra of HA and m-DOM

	region	vibrational assignment
I O-H and N-H st		O-H and N-H stretching modes
	II	aliphatic C-H stretching mode
	III	C=O stretching mode of carboxylic acids, aldehydes, and ketones
	IV	C=O stretching motion of quinones and amide I, C=N of imines and C=C of alkenes or aromatics
	V	ring breathing mode of aromatics and C-H and O-H bending modes
	VI	C-O stretching mode of phenol and alcohols and O-H bending modes of carboxylic acids
	VII	C-O stretching mode of polysaccharide-like substances and C-H in-plane bending mode of aromatics

Figure 3A shows the ATR-FTIR spectrum of commercial HA with assignments based on relevant literature. 21-26 The broad peak in region I ranging from ca. 3400 to 3000 cm<sup>-1</sup> is due to O-H and N-H stretching modes. The broad nature of the absorption and the fact that it extents to lower wavenumber values is evidence that there is considerable hydrogen bonding. The absorptions in region II with peak maxima at 2920 and 2850 cm<sup>-1</sup> are indicative of aliphatic CH<sub>2</sub> and CH3 stretching modes, respectively. The absorption in region III centered at 1709 cm<sup>-1</sup> is due to C=O vibrations of carboxylic acids, aldehydes, and ketones. Region IV has an absorption near 1629 cm<sup>-1</sup> that can be attributed to a number of species and combinations thereof, including aromatic moieties and olefinic C=C and C-C vibrations, C=N aliphatic imines, and C=O stretching of quinones. Other lower wavenumber absorptions for HA (below 1630 cm<sup>-1</sup>) suggest the presence of aromatic moieties as a result of ring vibrational modes. The absorption near 1408 cm<sup>-1</sup> in spectral

region V also indicates aromaticity, because it can be attributed to aromatic ring absorption modes as well as deformation of aliphatic C–H and O–H in phenols and alcohols. The broad doublet in region VI around 1227 cm $^{-1}$  is possibly due to O–H stretching of phenols and alcohols as well as C–O stretching and O–H deformation of carboxylic acids. Region VII has absorptions around 1032 cm $^{-1}$  from C–O stretching of polysaccharide-like structures and in-plane C–H bending of the benzene ring as well as peaks at  $\sim$ 915 cm $^{-1}$  as a result of aromatic out-of-plane C–H bends.

The same type of analysis for HA can be applied to mcDOM (Figure 3B). The relative contributions and presence or absence of key absorptions reveal clear differences between m-cDOM and HA. First, there is a larger contribution near 3279 cm<sup>-1</sup> in region I compared to the HA spectrum, indicating a greater contribution of O-H and N-H groups. Furthermore, the aliphatic C-H stretching absorptions in region II are less intense. The absorption at 1707 cm<sup>-1</sup> is broader, suggesting contributions from different types of molecular species containing the carbonyl group. Unlike HA, there is no isolated absorption at 1629 cm<sup>-1</sup>. Instead, the absorption at 1709 cm<sup>-1</sup> is broadened with a shoulder. This difference, in addition to the larger peak observed in region I, points toward the presence of nitrogen-containing groups, such as amides and amines. Furthermore, the lack of a feature at 1629 cm<sup>-1</sup> suggests less aromatic species. Taken together, these results indicate that the m-DOM sample is likely more oxidized and non-aromatic and has an abundance of nitrogencontaining functional groups, while HA contains an abundance of aromatic species with high degrees of carboxylic acid functional groups. These results are in general agreement with the EEM analysis as well MS analysis (vide infra).

HESI-LIT-Orbitrap MS Analysis. Figure 4 shows the contribution of molecular species in HA and m-DOM based on analysis upon direct injection of each sample into HESI-LIT-Orbitrap MS. Immediately apparent is the fact that the m-DOM sample is much more chemically complex than the HA sample. A total of 3496 species were identified for m-DOM compared to just 684 for HA. The average O/C ratio of m-DOM is 0.30 compared to 0.2795 for HA (Table 3). Figure 4 also shows that m-DOM has more nitrogen-containing species than HA (60 versus 39% of total identified formulas,

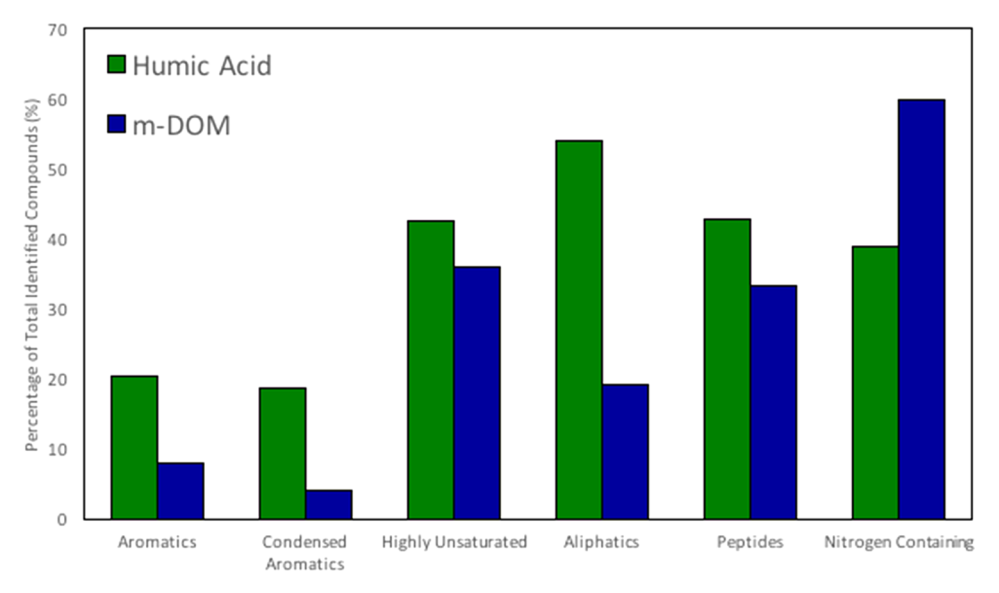


Figure 4. Relative abundance of each molecular class in HA and m-DOM as determined by HESI-LIT-Orbitrap MS analysis calculated according to the Experimental Procedures.

Table 3. Molecular Characteristics of HA and m-DOM as Determined by HESI-LIT-Orbitrap MS Analysis

	m-DOM	HA
all formulas	3496	684
average AI	0.14	0.19
average H/C	1.57	1.56
average O/C	0.30	0.28

respectively) and is less aromatic (12 versus 38%, respectively). The fraction of nitrogen-containing species observed in our HA sample agrees will with a previous study that analyzed groundwater DOM and found that 15-38% of identified species contained nitrogen.<sup>27</sup> Furthermore, the higher fraction of CHON species in m-DOM compared to terrestrial DOM in our study is in agreement with a previous experiment, in which both terrestrial and marine DOM were directly compared. 16 Interestingly, both m-DOM and HA have high percentages of highly unsaturated species (36 and 41%). Previous studies have identified the main contributors to the "highly unsaturated" category as either carboxylic-rich alicyclic molecules (CRAM) formed from autochthonous microbial sources or aromatic lignin from terrestrial sources.<sup>17</sup> Given that the m-DOM was produced in a laboratory without input from terrestrial sources, it is more likely the highly unsaturated species are due to CRAM molecules, while the highly unsaturated species in HA are from lignin. This would again explain the differences in the impact of m-DOM as a photosensitizer, because CRAM is less photoactive than lignin, which is highly aromatic. Overall, the results from MS analysis agree with the ATR-FTIR and EEM spectra of these two complex systems, which show that m-DOM is more oxygenated and less aromatic and has more nitrogen-containing species.

## CONCLUSION

In this study, we compared the three different potential photosensitizers with increasing chemical complexity (i.e., BBA, HA, and m-DOM) to initiate photosensitized reactions with the fatty acid NA in an organic-rich environment. ATR—FTIR and HRMS results revealed that BBA is an efficient photosensitizer, leading to the production of several unsatu-

rated and functionalized products, including saturated and unsaturated  $C_8$  aldehydes/ketones, combination products (BBA + NA), and hydroxy-NA. HA was found to be a less efficient photosensitizer than BBA yet still produced similar unsaturated and functionalized products. Irradiation of NA in the presence of m-DOM led to no enrichment of condensed-phase products, indicating the m-DOM and associated chromophores produced by marine microbes appear to be less efficient photosensitizers within a rich organic layer.

Analysis of HA and m-DOM by EEMs, ATR-FTIR, and HESI-LIT-Orbitrap MS reveals that HA is photoactive as a result of its presence of aromatic species, while m-DOM was less photoactive as a result of its high abundance of CRAM, which is less aromatic. Interestingly, despite its lower photoreactivity with NA, the m-DOM still appeared to undergo photochemistry itself, an avenue that should be investigated further in future studies.

It should be noted that, while this study points toward the lower activity in these photosensitized reactions for microbially produced DOM, it does not preclude the importance of such reactions at the surface of the open ocean or at the surface of SSA altogether, because other sources of CDOM in these regions exist. For example, previous work has shown that highly chromophoric dissolved polycyclic aromatics are formed thermogenically in the deep ocean.<sup>26</sup> Furthermore, terrestrial input of photoactive lignin-type molecules can also add to the number of chromophores found at the air-water interface of the ocean in coastal regions. 28 Finally, the production of DOM in the real ocean system is a highly complex process that includes a range of factors that may not be accounted for here. Future studies should further investigate the photoreactivity ability of freshly upwelled deep water DOM and coastal region DOM as well as work toward understanding the chemical composition and characteristics of marine-derived DOM under varying microbial conditions.

Additional consideration regarding the scope of the current study should be given with respect to differences between laboratory studies and that which occurs in the environment. While these results lend credence to the idea that the thin films used in our study are accurate mimics of interfacial systems,

future studies should be conducted to determine if the photochemical products of condensed and gaseous products at aqueous surfaces coated with organic films and photosensitizer could be useful and provide additional instights into photochemistry in marine environments. Overall, the findings in this study are important in that they lend further knowledge of the variability of DOM from various sources (here, m-DOM) to serve as a photosensitizer. These results point toward the need for studies using complex, authentic model systems in such experiments to further our understanding of different photochemical processes occurring in marine environments.

# ASSOCIATED CONTENT

# Supporting Information

The Supporting Information is available free of charge on the ACS Publications website at DOI: 10.1021/acsearthspace-chem.9b00066.

ATR-FTIR spectra of thin films of each of the photosensitizer used in this study (Figure S1), ATR-FTIR spectra of NA alone and with each of the photosensitizers used in this study (Figure S2), peak assignments for NA (Table S1), ATR-FTIR difference spectra of irradiated NA and m-DOM alone (Figure S3), signal detected (counts) for select products analyzed by HESI-LIT-Orbitrap MS for control NA and NA with BBA (Figure S4), and signal detected (counts) for select products analyzed by HESI-LIT-Orbitrap MS analysis (Figure S5) (PDF)

#### AUTHOR INFORMATION

### **Corresponding Author**

\*Telephone: 858-534-2499. E-mail: vhgrassian@ucsd.edu.

ORCID ®

Richard E. Cochran: 0000-0002-0736-6529 Vicki H. Grassian: 0000-0001-5052-0045

# **Author Contributions**

<sup>†</sup>Jonathan V. Trueblood and Michael R. Alves contributed equally to this work.

#### Notes

The authors declare no competing financial interest.

# ■ ACKNOWLEDGMENTS

The authors gratefully acknowledge support by the National Science Foundation through the Center for Aerosol Impacts on Chemistry of the Environment funded under the Centers for Chemical Innovation Program Grant CHE1801971. The authors also thank Professor Michael Tauber and Samantha Doyle for m-DOM sample preparation and extraction.

## REFERENCES

- (1) Thurman, E. M. Organic Geochemistry of Natural Waters; Springer: Dordrecht, Netherlands, 1985; p 497, DOI: 10.1007/978-94-009-5095-5.
- (2) Timko, S. A.; Maydanov, A.; Pittelli, S. L.; Conte, M. H.; Cooper, W. J.; Koch, B. P.; Schmitt-Kopplin, P.; Gonsior, M. Depth-Dependent Photodegradation of Marine Dissolved Organic Matter. *Front. Mar. Sci.* **2015**, 2 (66), 1–13.
- (3) Vione, D.; Calza, P. Introduction. In *Surface Water Photochemistry*; Calza, P., Vione, D., Eds.; Royal Society of Chemistry: Cambridge, U.K., 2015; Chapter 1, pp 1–15, DOI: 10.1039/9781782622154-00001.

I

- (4) Canonica, S. Oxidation of Aquatic Organic Contaminants Induced by Excited Triplet States. *Chimia* **2007**, *61* (61), 641–644.
- (5) McNeill, K.; Canonica, S. Triplet State Dissolved Organic Matter in Aquatic Photochemistry: Reaction Mechanisms, Substrate Scope, and Photophysical Properties. *Environ. Sci. Process. Impacts* **2016**, *18* (11), 1381–1399.
- (6) Clark, C. D.; Zika, R. G. Marine Organic Photochemistry: From the Sea Surface to Marine Aerosols. In *Marine Chemistry*. *The Handbook of Environmental Chemistry*; Wangersky, P. J., Ed.; Springer-Verlag: Berlin, Germany, 2000; Vol. *SD*, pp 1–33, DOI: 10.1007/10683826 1.
- (7) Ciuraru, R.; Fine, L.; Van Pinxteren, M.; D'Anna, B.; Herrmann, H.; George, C. Photosensitized Production of Functionalized and Unsaturated Organic Compounds at the Air-Sea Interface. *Sci. Rep.* **2015**, *5* (1), 12741.
- (8) Ciuraru, R.; Fine, L.; van Pinxteren, M.; D'Anna, B.; Herrmann, H.; George, C. Unravelling New Processes at Interfaces: Photochemical Isoprene Production at the Sea Surface. *Environ. Sci. Technol.* **2015**, *49* (22), 13199–13205.
- (9) Fu, H.; Ciuraru, R.; Dupart, Y.; Passananti, M.; Tinel, L.; Rossignol, S.; Perrier, S.; Donaldson, D. J.; Chen, J.; George, C. Photosensitized Production of Atmospherically Reactive Organic Compounds at the Air/Aqueous Interface. *J. Am. Chem. Soc.* **2015**, 137 (26), 8348–8351.
- (10) Tinel, L.; Rossignol, S.; Bianco, A.; Passananti, M.; Perrier, S.; Wang, X.; Brigante, M.; Donaldson, D. J.; George, C. Mechanistic Insights on the Photosensitized Chemistry of a Fatty Acid at the Air/Water Interface. *Environ. Sci. Technol.* **2016**, *50* (20), 11041–11048.
- (11) Hansell, D.; Carlson, C.; Repeta, D.; Schlitzer, R. Dissolved Organic Matter in the Ocean: A Controversy Stimulates New Insights. *Oceanography* **2009**, 22 (4), 202–211.
- (12) Nelson, N. B.; Siegel, D. A. The Global Distribution and Dynamics of Chromophoric Dissolved Organic Matter. *Annu. Rev. Mar. Sci.* **2013**, 5 (1), 447–476.
- (13) Coble, P. G. Marine Optical Biogeochemistry: The Chemistry of Ocean Color. *Chem. Rev.* **2007**, *107* (2), 402–418.
- (14) Dittmar, T.; Koch, B.; Hertkorn, N.; Kattner, G. A Simple and Efficient Method for the Solid-Phase Extraction of Dissolved Organic Matter (SPE-DOM) from Seawater. *Limnol. Oceanogr.: Methods* **2008**, 6 (6), 230–235.
- (15) Koch, B. P.; Witt, M.; Engbrodt, R.; Dittmar, T.; Kattner, G. Molecular Formulae of Marine and Terrigenous Dissolved Organic Matter Detected by Electrospray Ionization Fourier Transform Ion Cyclotron Resonance Mass Spectrometry. *Geochim. Cosmochim. Acta* 2005, 69 (13), 3299–3308.
- (16) Kujawinski, E. B.; Longnecker, K.; Blough, N. V.; Del Vecchio, R.; Finlay, L.; Kitner, J. B.; Giovannoni, S. J. Identification of Possible Source Markers in Marine Dissolved Organic Matter Using Ultrahigh Resolution Mass Spectrometry. *Geochim. Cosmochim. Acta* **2009**, 73 (15), 4384–4399.
- (17) Stubbins, A.; Dittmar, T. Illuminating the Deep: Molecular Signatures of Photochemical Alteration of Dissolved Organic Matter from North Atlantic Deep Water. *Mar. Chem.* **2015**, *177*, 318–324.
- (18) Rapf, R. J.; Perkins, R. J.; Carpenter, B. K.; Vaida, V. Mechanistic Description of Photochemical Oligomer Formation from Aqueous Pyruvic Acid. *J. Phys. Chem. A* **2017**, *121* (22), 4272–4282.
- (19) Wang, Z.; Sun, J.; Xie, S.; Ma, G.; Jia, Y. Thermal Properties and Reliability of a Lauric Acid/Nonanoic Acid Binary Mixture as a Phase-Change Material for Thermal Energy Storage. *Energy Technol.* **2017**, *5* (12), 2309–2316.
- (20) Stuart, B. H. Infrared Spectroscopy: Fundamentals and Applications; John Wiley and Sons, Ltd.: Chichester, U.K., 2004; DOI: 10.1002/0470011149.
- (21) Smith, B. Infrared Spectral Interpretation: A Systematic Approach; CRC Press (Taylor & Francis Group): Boca Raton, FL, 1999.
- (22) Coates, J. Interpretation of Infrared Spectra, A Practical Approach. In *Encyclopedia of Analytical Chemistry*; Meyers, R. A., Ed.; John Wiley and Sons, Ltd.: Chichester, U.K., 2006; DOI: 10.1002/9780470027318.a5606.

- (23) Pospíšilová, L.; Fasurova, N. Spectroscopic Characteristics of Humic Acids Originated in Soils and Lignite. *Soil Water Res.* **2009**, *4* (4), 168–175.
- (24) Tatzber, M.; Stemmer, M.; Spiegel, H.; Katzlberger, C.; Haberhauer, G.; Mentler, A.; Gerzabek, M. H. FTIR-Spectroscopic Characterization of Humic Acids and Humin Fractions Obtained by Advanced NaOH, Na<sub>4</sub>P<sub>2</sub>O<sub>7</sub>, and Na<sub>2</sub>CO<sub>3</sub> Extraction Procedures. *J. Plant Nutr. Soil Sci.* **2007**, 170 (4), 522–529.
- (25) Ribeiro, J. S.; Ok, S. S.; Garrigues, S.; De la Guardia, M. FTIR Tentative Characterization of Humic Acids Extracted from Organic Materials. *Spectrosc. Lett.* **2001**, 34 (2), 179–190.
- (26) Dittmar, T. The Molecular Level Determination of Black Carbon in Marine Dissolved Organic Matter. *Org. Geochem.* **2008**, 39 (4), 396–407.
- (27) Longnecker, K.; Kujawinski, E. B. Composition of Dissolved Organic Matter in Groundwater. *Geochim. Cosmochim. Acta* **2011**, 75, 2752–2761.
- (28) Stubbins, A.; Spencer, R. G. M.; Chen, H.; Hatcher, P. G.; Mopper, K.; Hernes, P. J.; Mwamba, V. L.; Mangangu, A. M.; Wabakanghanzi, J. N.; Six, J. Illuminated Darkness: Molecular Signatures of Congo River Dissolved Organic Matter and Its Photochemical Alteration as Revealed by Ultrahigh Precision Mass Spectrometry. *Limnol. Oceanogr.* **2010**, *55* (4), 1467–1477.